Journal of ELECTRONIC MATERIALS, Vol. 45, No. 7, 2016
DOI: 10.1007/s11664-016-4498-1
© 2016 The Author(s). This article is published with open access at Springerlink.com

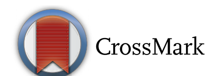

Contact Resistance and Metallurgical Connections Between Silver Coated Polymer Particles in Isotropic Conductive Adhesives

SIGURD R. PETTERSEN,[1] HELGE KRISTIANSEN,[1,2] SHIJO NAGAO,[3] SUSANNE HELLAND,[4] JOHN NJAGI,[5] KATSUAKI SUGANUMA,[3] ZHILIANG ZHANG,[1] and JIANYING HE[1,6]

1.—NTNU Nanomechanical Lab, Department of Structural Engineering, Norwegian University of Science and Technology (NTNU), 7491, Trondheim, Norway. 2.—Conpart AS, 2013, Skjetten, Norway. 3.—Institute of Scientific and Industrial Research (ISIR), Osaka University, Ibaraki, Osaka 567-0047, Japan. 4.—Mosaic Solutions AS, 2013, Skjetten, Norway. 5.—Center for Advanced Materials Processing, Clarkson University, Potsdam, NY 13699-5814, USA. 6.—e-mail: jianying.he@ntnu.no

Recently, there has been an increasing interest in silver thin film coated polymer spheres as conductive fillers in isotropic conductive adhesives (ICAs). Such ICAs yield resistivities similar to conventional silver flake based ICAs while requiring only a fraction of the silver content. In this work, effects of the nanostructure of silver thin films on inter-particle contact resistance were investigated. The electrical resistivity of ICAs with similar particle content was shown to decrease with increasing coating thickness. Scanning electron micrographs of ion milled cross-sections revealed that the silver coatings formed continuous metallurgical connections at the contacts between the filler particles after adhesive curing at 150°C. The electrical resistivity decreased for all samples after environmental treatment for 3 weeks at 85°C/85% relative humidity. It was concluded that after the metallurgical connections formed, the bulk resistance of these ICAs were no longer dominated by the contact resistance, but by the geometry and nanostructure of the silver coatings. A figure of merit (FoM) was defined based on the ratio between bulk silver resistivity and the ICA resistivity, and this showed that although the resistivity was lowest in the ICAs containing the most silver, the volume of silver was more effectively used in the ICAs with intermediate silver contents. This was attributed to a size effect due to smaller grains in the thickest coating.

Key words: Conductive adhesives, contact resistance, metallic contacts, silver thin films, metal-coated polymer particles, size-dependent resistivity

INTRODUCTION

As lead-based solders are banned in a growing range of products due to environmental concerns, isotropic conductive adhesives (ICAs) are emerging as a promising alternative in electronic interconnects because of advantages such as lower processing temperatures and fewer processing steps compared to lead-free solders.[1] Conventionally, ICAs comprises micron-sized silver flakes embedded in an adhesive matrix, normally a thermosetting epoxy system. An interconnecting network of silver flakes makes the ICA electrically conductive,

Sigurd R. Pettersen: Parts of this work were done during an academic stay at Institute of Scientific and Industrial Research (ISIR), Osaka University, Ibaraki, Osaka 567-0047, Japan
(Received December 14, 2015; accepted March 24, 2016; published online April 19, 2016)

whereas the epoxy matrix provides structural integrity and adhesion. Even with the large surface-to-volume ratio of silver flakes, the amount of silver must be relatively large to achieve sufficient electrical conductivity; typically a volume fraction of 25–30% is required, corresponding to a weight fraction of 70–80%. This large fraction of precious metal severely affects the cost-efficiency of ICAs, and increases the impact of undesirable material properties such as brittleness and thermal expansion mismatch between the components.

Replacing the silver flakes with micron-sized polymer spheres coated with tens to hundreds of nanometres silver (AgPS) can significantly reduce the amount of precious metal required to obtain satisfactory electrical conductivity. Figure 1 shows a cross-section of such an AgPS-based ICA, containing a volume fraction of about 56% AgPS but less than 3% silver. Similar ICAs have been shown to exhibit resistivities lower than 10^{-3} Ω cm; a value in the same range as that of conventional flake-based ICAs, which contain about ten times the volume fraction of silver.[1,2] By tailoring the size and composition of the polymer cores, material property mismatch between the filler particles and epoxy matrix can be reduced. Nguyen et al. investigated the die shear strength of AgPS-based ICA and found it to be larger than both in-house produced and commercial flake-based ICAs.[3] The rheological properties of these ICAs have also been investigated and deemed suitable for stencil/screen printing and dispensing processes.[4] Gakkestad et al. investigated the thermal properties of AgPS-based ICAs.[2] A thermal conductivity of 1 W/m K was obtained at approximately 1.4 vol.% silver, whereas a flake-based ICA required 16 vol.% silver to reach the same value. Jain et al. explored the effect of various AgPS sizes, volume fractions, epoxy types and curing conditions, and coating thickness on electrical properties of these ICAs.[5–7] The resistivities of ICAs containing 30 μm AgPS with 100 nm, 150 nm, 200 nm, and 250 nm silver coatings were measured over a range of particle volume fractions.[7] In general, it was found that for the same particle volume fraction, ICAs containing AgPS with thicker coatings yielded higher conductivities.

The conductivity of conventional ICAs is often explained by percolation theory, where at a critical volume fraction of filler particles, enough inter-particle contacts are formed to create at least one complete conduction path.[1] As the filler concentration increases above this percolation threshold, the number of contacts rapidly increases to form a network of parallel conductors, where each conductor can be seen as a number of resistors in series. These resistors can be divided in two categories: the bulk resistance from the conductive filler particles, which is dependent on the resistivity and geometry of the particles, and the inter-particle contact resistance. In conventional ICAs, the contact resistance is generally regarded as the dominating factor.[8,9] In addition to a concentration of conductive fillers above the percolation threshold, most ICAs require curing to lower the resistivity to an acceptable level. Curing leads to cross-linking and shrinkage in the epoxy matrix, which presses the particles together, decreasing the contact resistance.[9]

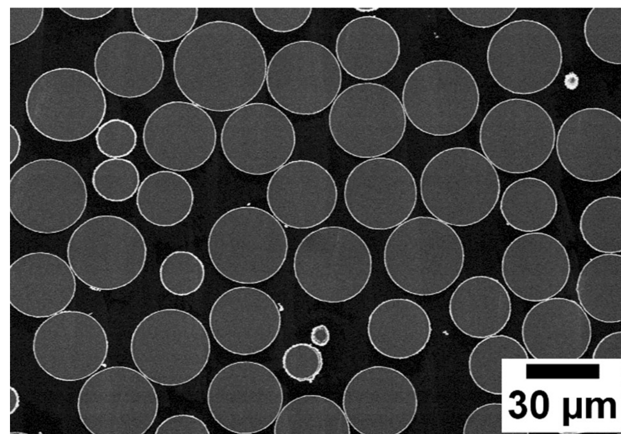

Fig. 1. FE-SEM image of a cross-sectioned ICA sample containing a volume fraction of 56% AgPS. PMMA particles (light grey) with a diameter of 30 μm are coated with 270 nm thick silver films (white) and embedded in an epoxy matrix (dark grey). The seemingly large size distribution is a result of the cross-section cutting through different planes in the randomly dispersed particles.

Constriction resistance and tunnelling resistance are the two main mechanisms behind the contact resistance, as described by Holm's classical contact theory.[10] If the contact areas are smaller than the cross-sectional areas of the particles, the flow of current will be narrowed, leading to a constriction resistance through the contacts. The resistance effect due to lattice mismatch between two metallic contact members in direct contact is similar to the resistance from the grain boundaries in a polycrystalline material. Even if there is no direct metallic contact, e.g. due to the presence of a thin polymer or oxide film, electrons may pass across the contact by quantum tunnelling. This effect is only dependent on the thickness of the insulating layer; the tunnelling decreases rapidly as the thickness increases, and at around 10 nm the tunnelling resistance is so large that tunnelling current is negligible.

In this work, we found that the resistivities of AgPS-based ICAs with similar volume fractions of particles decreased exponentially with increasing coating thickness. High resolution scanning electron microscope (SEM) imaging of cross-sectioned samples revealed that the intermediate to thickest coatings had formed metallurgical contacts. The impact of these contact structures on the conductive properties of AgPS-based ICAs are discussed, and it is concluded that the contact resistance mechanisms assumed to dominate in conventional ICAs are negligible as long as the metallurgical contacts are formed. The formation of such metallurgical

contacts thus helps explain the good conductive properties relative to the low silver content exhibited by AgPS-based ICAs.

MATERIALS AND METHODS

Sample Preparation

Poly(methyl methacrylate) (PMMA) spheres with a diameter of 30 μm (coefficient of variation $\leq$5%) and nominal silver coating thicknesses of 60 nm, 100 nm, 150 nm, and 270 nm were provided through Mosaic Solutions AS (Skjetten, Norway). The coating was applied by an electroless plating procedure, and the coating thicknesses were estimated from the amount of silver used in the coating process, assuming that all the silver was incorporated in the coatings. Representative particles with each coating thickness can be observed in Fig. 2. The density of the polymer cores was given by the manufacturer as 1.16 g/cm^3, and the densities of the silver coatings were assumed to be equal to that of bulk silver (10.49 g/cm^3). The epoxy matrix was prepared by mixing a low viscosity epoxy resin consisting of a mixture of bisphenol A and bisphenol F epoxy with a low viscosity polyetheramine curing agent at a ratio of 1:0.35 by weight. The uncured densities of the resin and curing agent were given by the manufacturer as 1.18 g/cm^3 and 0.95 g/cm^3, respectively. Particles were mixed into the epoxy at a volume fraction of approximately 56% using a centrifugal vacuum mixer (ARV-310, Thinky Corporation, Japan). The mixing was done in two steps: 2000 rpm for two min at atmospheric pressure, followed by 1000 rpm for four min at 0.3 kPa pressure to remove air from the samples. The ICA was screen printed into Teflon moulds with dimensions 10 mm $\times$ 10 mm $\times$ 1 mm, and cured at 150°C for 30 min. The moulds confined potential flow of the uncured ICAs, thus minimizing influence of the different coating surfaces on the rheological behaviour of the ICAs. The four ICA series are denoted 60Ag, 100Ag, 150Ag, and 270Ag, respectively. The calculated particle and silver content of the series can be found in Table I.

Electrical 4-Pin Measurements

The electrical volume resistivity was measured with a 4-pin setup (Loresta-GP MCP-T610 with a 4-pin NSCP probe, Mitsubishi Chemical Analytech, Japan) on six samples from each ICA series. The probe had a built-in spring system, ensuring equal contact pressure on the samples in each measurement. The thickness of each sample was measured with a digital calliper, and the instrument automatically calculated the resistivity for each measurement by multiplying the resistance with the thickness and a resistivity correction factor (RCF). The RCF corrected for restrictions imposed on the electrical field by the sample size and geometry, as well as the probe position. The resistivities of the ICA series were averaged from eight measurements on each of the six samples from every series.

Harsh Environmental Testing

To investigate how the sample properties would change after a harsh environment test, the samples were placed in an environmental chamber (Espec SH-240 temperature and humidity chamber, Espec Corporation, Japan) at 85°C and 85% relative humidity (RH) for 3 weeks. After the environmental test, the samples were dried in ambient conditions for at least 48 h before the electrical resistivity was measured following the same procedure. The data sets from before and after the environmental test are denoted *pre-ET* and *post-ET*, respectively.

Polishing and FE-SEM Imaging of ICA Cross-Sections

To investigate the structure of the silver coatings at the various thicknesses, both *pre-ET* and *post-ET* samples from the four ICA series were cross-sectioned and further imaged by field emission scanning electron microscopy (FE-SEM). The samples were first mechanically polished with SiC paper (#4000 from Struers; grain size 5 μm) at 150 rpm to get cross-sections a certain distance into the bulk of the samples. A segment of each cross-section was further ion milled by argon ions at 6 kV for approx. 3–5 h using an ion milling system in cross-sectional milling mode (IM4000, Hitachi High-Technologies Co., Ltd. Japan). The cross-sections were imaged by field emission SEM (SU8020, Hitachi High-Technologies Co., Ltd. Japan) at an acceleration voltage of 2 kV.

RESULTS

Electrical Resistivity

With the exception of the ICA series with the thinnest coating before the environmental chamber test (60Ag *pre-ET*), the spread in resistivity values within each series was small. There is a clear trend that the resistivity of the ICA decreased as the estimated silver content increased, as can be observed in Fig. 3. The lowest average resistivity value was found for the 270Ag *post-ET* series, at $6.7 \times 10^{-4} \pm 0.5 \times 10^{-4}$ Ω cm. The other striking feature is the decrease in resistivity for the samples after 3 weeks at 85°C and 85%RH, most obvious in the 60Ag series. As the electrical measurements were conducted on the same samples *pre-* and *post-ET*, this large decrease in both spread and average resistivity for the samples with the thinnest coatings suggest that a significant structural change occurred in these samples during the environmental treatment. Before the environmental treatment, the coefficient of variation (CV) was 77% for the 60Ag series, and this decreased to 7% *post-ET*. For the 100Ag, 150Ag, and 270Ag series, the CV decreased

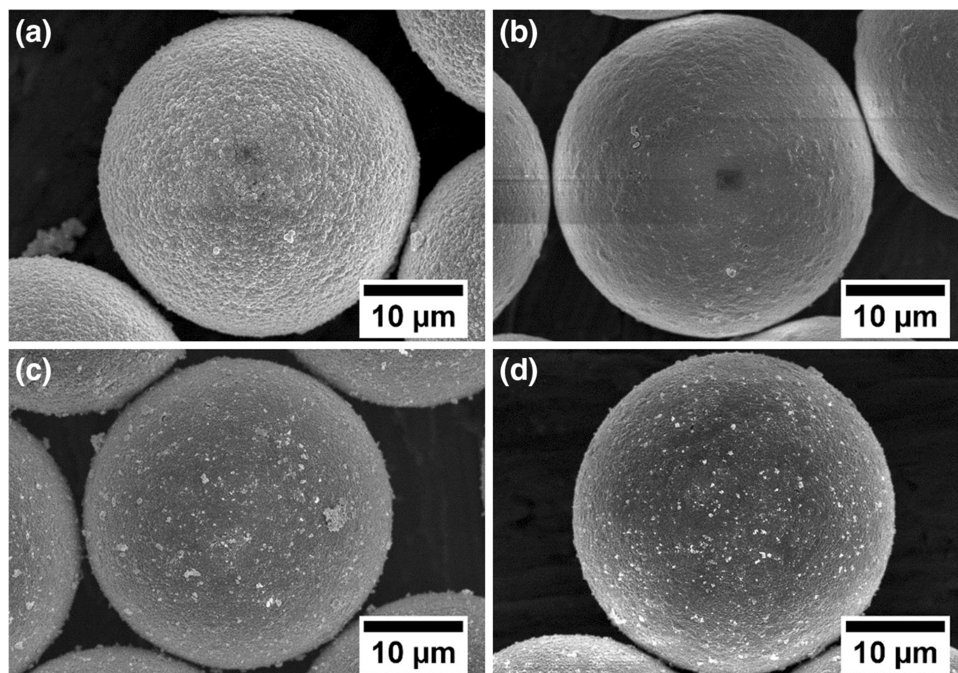

Fig. 2. Representative particles with nominal coating thicknesses of 270 nm (a), 150 nm (b), 100 nm (c), and 60 nm (d), respectively. Each particle is covered by a continuous film of silver, made up of nodular grain structures.

Table I. Particle, volume, and mass fractions of the four ICA series, calculated from the measured weights, as well as densities and dimensions given by Mosaic Solutions

Series	Nominal coating thickness (nm)	Volume fraction particles (%)	Volume fraction silver (%)	Mass fraction silver (%)
60Ag	60	56.0	0.7	5.8
100Ag	100	56.1	1.1	9.3
150Ag	150	56.5	1.7	13.4
270Ag	270	56.4	2.9	21.8

Calculations are based on uncured density values.

from 11% to 8%, 14% to 10%, and 9% to 7%, respectively.

Cross-Sectional FE-SEM Images

Contact Zones

As the AgPS are randomly dispersed in the epoxy matrix, an arbitrary cross-section may cut through all possible normal planes along the particle diameters. Even with a large estimate for the contact diameter, e.g. 1 μm, only about 3% of all possible arbitrary cross-sections along the particle diameter pass through the contact zones. The small interparticle contact zones will, therefore, not be observable for most particles in an arbitrary cross-section through the ICA. Even though it looks like many of the particles are in contact in Fig. 1, increasing the magnification reveals that most particles in the cross-sections are separated by tens to hundreds of nanometers of epoxy. For particles where the cross-sections went through the contact zones, the polycrystalline grain structure was continuous over the contact zone, forming an uninterrupted metallurgical connection between the particles. The exception was the *pre-ET* 60Ag series, where no such metallurgical contacts were observed. In the *post-ET* 60Ag series, metallurgical contacts were present similar as in the series with thicker coatings. Representative cross-sections of the contact zones of the four ICA series can be seen for *pre-ET* samples in Fig. 4 and for *post-ET* samples in Fig. 5.

Grain Size

By directly measuring the widths of grain cross-sections, it can be observed that many grains were smaller than 50 nm for the 60 nm coatings. It should be noted that this procedure may

underestimate the grain size, as an arbitrary cross section can pass through all cut planes along a grain and not only where the grains are at their widest. The relative grain size seemed to increase for the 100 nm and 150 nm coatings. The 270 nm coatings on the other hand contained more small grains than the two coatings of intermediate thicknesses, but the thickest coatings also encompassed many abnormally large grains with cross-sectional widths of several hundred nanometres. After storage at 85°C/85% RH, these abnormally large grains were even more prominent.

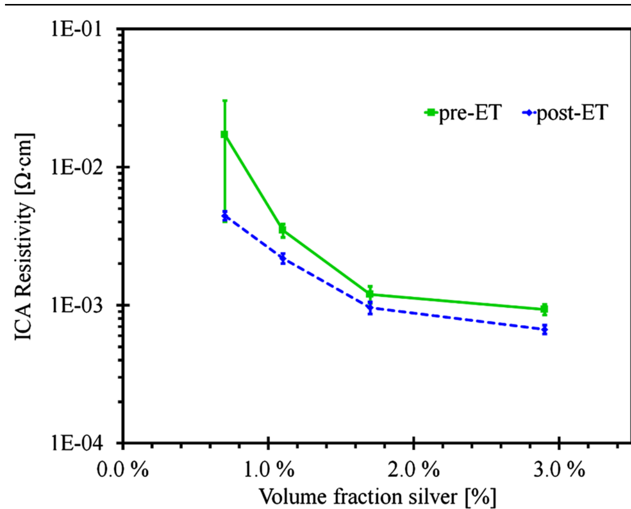

Fig. 3. Electrical resistivity of the four ICA series before (*pre-ET*) and after (*post-ET*) storage for 3 weeks 85°C and 85%RH, averaged from 48 measurements on six samples for each series. The error bars show ± one standard deviation.

DISCUSSION

Conduction and Resistance Mechanisms In AgPS-Based ICAs

Varying Coating Thickness

The electrical conduction in the AgPS-based ICAs requires a combination of conduction in the metal coatings and contacts between the particles. Both are expected to contribute to the resistivity of the ICA. The resistivities shown in Fig. 3 are calculated based on the bulk dimensions of the ICA samples. At about 56%, the volume fraction of particles was well above the percolation limit, which for 30 μm AgPS have been reported to be around 35%, with a slight dependence on coating thickness.[7] The particle volume fraction was almost identical in all four ICA series, and the number of potential parallel conducting pathways should thus be similar in all samples. As a first order estimate, it can be assumed that the conductive fraction of a cross-sectional area of the ICA will be equal to the volume fraction of silver. Increasing the silver coating thickness thus increases the total cross-sectional area of the parallel conducting pathways of the ICA samples. Effective resistivities for the different silver coating thicknesses can, therefore, be calculated by multiplying the measured resistivity of the ICAs by the volume fraction of silver. Figure 6 shows such effective resistivity values, where the ICA

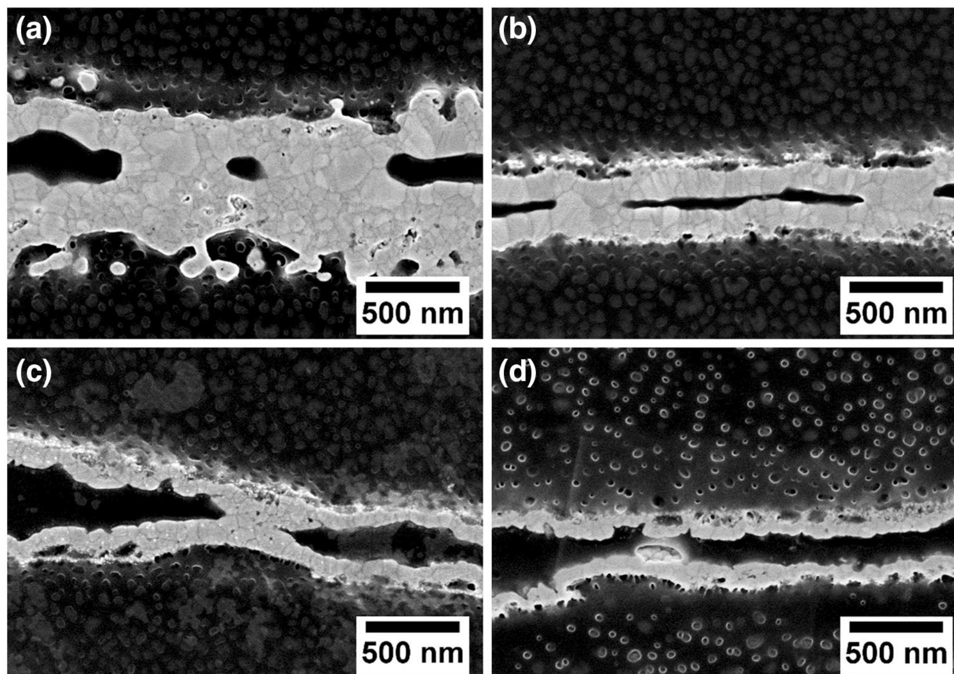

Fig. 4. Representative cross-sections of contact zones between two particles from 270Ag (a), 150Ag (b), 100Ag (c), and 60Ag (d) *pre-ET* ICA series, respectively. In the three thickest coatings, the metallurgic connections were observable in the contact zones. For the 60Ag *pre-ET* series, no such continuous contacts were observed.

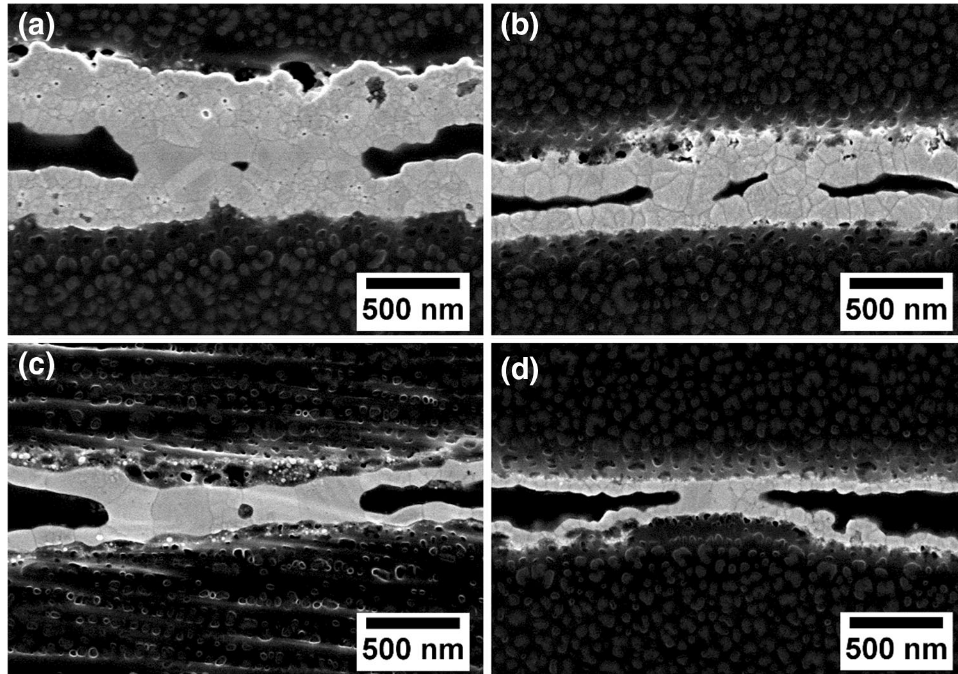

Fig. 5. Representative cross-sections of contact zones between two particles from 270Ag (a), 150Ag (b), 100Ag (c), and 60Ag (d) *post-ET* ICA series, respectively.

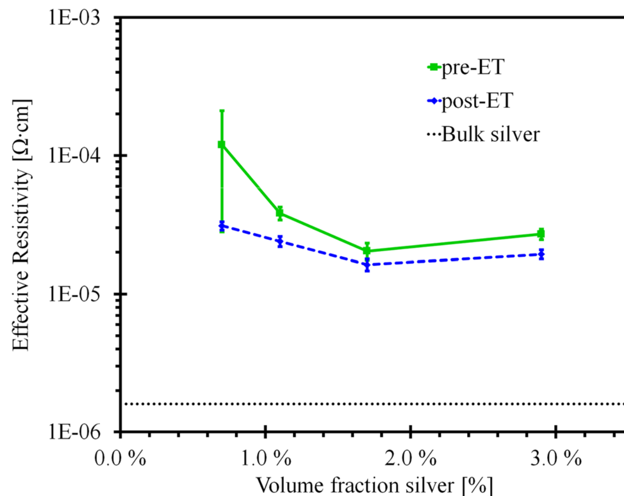

Fig. 6. Effective resistivity values for the conductive volume fraction of the four ICA series. Calculated by multiplying the measured ICA resistivity values before (*pre-ET*) and after (*post-ET*) storage for 3 weeks 85°C and 85%RH with the corresponding volume fractions of silver. The error bars show ± one standard deviation.

resistivity from each 4-pin measurement has been multiplied with the corresponding volume fraction of silver and further averaged for each ICA series.

By comparing the data in Figs. 6 to 3, it is clear that most of the differences in resistivity for the ICA series *post-ET* were due to the differing thickness of the silver coatings. However, it is obvious that also other factors influenced the ICA resistivity, especially for the *pre-ET* samples. If coating thickness was the only factor influencing the ICA resistivity, the effective values in Fig. 6 should be constant. Reasons for these deviations are discussed in the following sections. Additionally, a figure of merit (*FoM*) (1) can be defined based on the ratio between bulk silver resistivity and effective resistivity.

$$FoM_{\mathrm{ICA}} = \frac{\rho_{\mathrm{Met}}}{\rho_{\mathrm{ICA}} \times \Phi_{\mathrm{Met}}} \tag{1}$$

where ρ_{Met} is the bulk resistivity of the metal, ρ_{ICA} is the bulk resistivity of the adhesive and Φ_{Met} is the volume fraction of metal. Assessment of such values is a suitable method for characterizing and comparing the use of metal in the various ICAs, as an ICA in which the conductive volume fraction conducts current as well as bulk silver would yield a *FoM* value of 1. Calculated *FoM* values can be found in Table II, and reveal that although the lowest resistivity is achieved in the 270Ag ICAs, the volume of silver is more effectively utilized in the 150Ag series. For comparison, a good conventional flake-based ICA can be assumed to have a resistivity of about 2×10^{-4} Ω cm and a volume fraction of 25% silver. This yields a *FoM* value of 0.032, indicating that the utilization of silver is more effective in almost all the AgPS-based ICAs in the present study.

Inter-particle Contact Resistance

The values given in Figs. 3 and 6 are derived from measurements on the same samples *pre-* and *post-ET*, so the large decrease in resistivity and data spread for the ICA with the thinnest coatings

Table II. Figure of merit (*FoM*) values for the four ICA series, calculated from measured resistivities before (*pre-ET*) and after (*post-ET*) storage for 3 weeks 85°C and 85%RH

Series	*FoM* (*pre-ET*)	*FoM* (*post-ET*)
60Ag	0.01	0.05
100Ag	0.04	0.07
150Ag	0.08	0.10
270Ag	0.06	0.08

suggest that a substantial change occurred in the silver coating and/or the contacts between the particles as a consequence of the environmental exposure. This is supported by the SEM study of the ICA cross-sections, as the continuous metallurgical contacts observed in the 100Ag, 150Ag, and 270Ag series were not found in the 60Ag series before the environmental test. However, such metallurgical contacts were clearly observable in a sample from the 60Ag series after 3 weeks at 85°C/85%RH. These structures will have a large impact on the contact resistance between the particles, and it is reasonable that the absence of such contacts in the 60Ag *pre-ET* series would significantly increase the resistivity of this ICA. The classical contact resistance theory of Holm is based on two semi-infinite structures in contact through a small contact area.[10] In such structures the constriction resistance is caused by a local narrowing of the electrical field lines close to the contact. For a structure with a conductive shell and insulating core such as the AgPS, the constriction is caused by the decreasing cross-sectional area of the spherical coating as the current flows towards a contact. When the current reaches the contact zone, the electrical field lines bend and the current flows through the contact into the adjacent coating. If the contact zone has a radius larger than the coating thickness, and assuming that the whole contact area is in perfect metallic contact, the available area is actually such that the current may spread out through the contact. In addition, the effective length of the conductive path through the contact zone is in the same range as the thickness of the metal film. The radii of the observed metallurgical contacts were usually in the same range or wider than the film thicknesses. Some observed contact structures were narrower than this, but a random two-dimensional cross-section of a three-dimensional structure is not very likely to cut through the widest section of the structure, so the actual contacts may have been wider. Contrary to what expected from most other models for ICA resistance, it is clear that the resistance of these AgPS-based ICAs is not dominated by inter-particle contact resistance as long as these metallurgical contacts are formed. The main impact of further widening of the metallurgical contact areas will be a reduced constriction of the current flow and shorter conduction path in the coating, and not the lowered resistance in the actual contact zone. The appearance of these connections also suggests that any tunnelling contribution to the contact conductance is negligible.[10]

Coating Structure and Size Effects

The nature of the inter-particle contacts will have a large impact on the ICA resistivity, as discussed in the previous section, but as long as the metallurgical connections are present and have a radius larger than the coating thickness, the resistance contribution from these will be very small compared to the bulk coating resistance. As can be observed in Fig. 6, there was a decrease in effective resistivity with increasing coating thickness, even in the series where these metallurgical connections were present. The exception is the 270Ag series, where the effective resistivity increased slightly compared to the 150Ag series. Mayadas-Shatzkes theory predicts that for polycrystalline films where the grain size is close to or smaller than the bulk electron mean free path, scattering at the grain boundaries will have a significant contribution on the resistivity.[11] It could be observed directly from the SEM images that the thinnest coatings contained grains smaller than 52 nm, which is the mean free path length of electrons in bulk silver.[12] The 100Ag and 150Ag series also contained grains smaller than this threshold, although the average grain size seemed to increase with coating thickness for these. In contrast, the coatings of the 270Ag series were comprised of many grains smaller than the grains of the intermediate coating thicknesses, but at the same time this series contained the largest amount of abnormally large grains. Parts of the variation in the effective resistivity in Fig. 6 may originate from a size effect due to a decrease in the mean free path of the electrons. After the environmental test, even larger grains were observed, supporting grain growth as an explanation for the decreased resistivity in the *post*-ET samples. In previous work on AgPS-based ICAs, poor quality of the thinner coatings has been reported as a possible explanation for the higher resistivities of ICAs containing AgPS with thin coatings.[7] However, SEM observation of both individual particles and ICA cross-sections revealed that in this work, even the 60Ag particles are completely coated with silver, as can be observed in Fig. 2.

Mechanisms for Grain Growth and Metallurgical Contacts

Sintering of Nano-sized Grains

Sintering of nano-sized silver particles in conductive adhesives at 150°C, which also is the curing temperature used to prepare the ICA samples in this study, have been reported by several

authors.[13–15] However, the grain sizes observed in the SEM images were much larger than the particle sizes for which sintering at such low temperatures have been observed (below 20 nm), and thus the lowered sintering temperature of nanoparticles is not by itself a fully satisfactory explanation for the structural changes observed in the ICA samples in this study. Still, it should be noted that the grain sizes observed in the SEM images were those of already cured samples, and so the initial grain size of the silver coatings before curing may have been smaller.

Artefact Investigation

Images were acquired in the larger cross-sections only polished mechanically with SiC paper, and metallurgical contacts were observable also in these rougher areas. It cannot be ruled out that the metallurgical contacts in these regions were a result of plastic deformation due to the shear force from the mechanical polishing. However, as the average roughness of the SiC paper was 5 μm and the ion beam milled approximately 100 μm further down in the cross-sections, it is unlikely that the metallurgical contacts in the ion milled sections were caused by the mechanical polishing. To check if the metallurgical contacts could be a result of heating from the ion milling, a sample was ion milled with a metallic protective mask directly connecting the surface of the ICA with a continuously refilled reservoir of liquid nitrogen. The metallurgical contacts were present also in this sample cross-sectioned with cooling, supporting the assumption that these were not artefacts. However, these results still cannot completely rule out localized heating introduced by the ion beam, so this should be a subject for further investigations. It is also unlikely that these metallurgical contacts are artefacts from the coating procedure. The contacts seemed to occur between two fully formed coatings, where each coating displayed a thickness equal to the coating outside of the contacts. If the metallurgical connections were formed during the coating procedure, the film thickness through the metallurgical contacts should be significantly thinner and not the observed thickness of at least twice that of the coatings.

Thermal Expansion and Epoxy Shrinkage

Inter-particle pressures are expected to impact the formation of metallic contacts. Gakkestad and co-workers reported a linear coefficient of thermal expansion (CTE) of 203 ppm/K at 150°C for an ICA comprised of the same epoxy matrix, cured at the same conditions, and containing AgPS with the same PMMA cores as used in this work.[2] The authors found that ICAs with a volume fraction of 40% AgPS yielded similar CTE values as at 46%, which was identical as the CTE value of the epoxy matrix without particles. This suggests that the addition of AgPS have very little impact on the thermal expansion of the ICA. The reference linear CTE value for bulk PMMA above the glass transition temperature is 190 ppm/K, very close to that of the ICA at 150°C.[16] At approximately 19 ppm/K, the CTE of silver is just a fraction of the CTE of the polymers.[17] Moreover, the volume fraction of silver as well as the thickness of the coatings are small compared to that of the polymers, hence it is reasonable that the silver has a negligible impact on the thermal expansion of the ICA. If the thermal expansion of the epoxy matrix was much larger than that of the filler particles, this would be expected to draw the particles apart at elevated temperatures. As the thermal expansion of the PMMA cores is similar to that of the surrounding epoxy, such an effect should be negligible in these ICAs. Gakkestad and co-workers performed their measurements on already cured ICAs. During curing, we expect shrinkage of the ICA due to cross-linking of the epoxy matrix.[18] Shrinkage of the epoxy matrix in addition to thermal expansion of the PMMA cores will press the silver coatings into contact, and this inter-particle pressure should advance the formation of metallic contacts. As the ICAs cool down after curing, the PMMA cores and cured epoxy go through approximately the same degree of thermal retraction due to similar CTEs, and the inter-particle pressure is maintained. In addition, a compressive stress field will occur in the silver coatings that will press the grains together as long as the external pressure from the epoxy matrix is larger than the internal pressure from the PMMA cores. Oh et al. have done extensive research on the hillock or abnormal grain growth dynamics in sputtered Ag thin films due to stress migration.[19–22] When compressive stresses are induced in silver thin films, stress relaxation will lead to increased diffusion of silver atoms along the grain boundaries, which can cause grain growth on the film surfaces. A similar process may occur in the AgPS-based ICAs. As can be observed in Fig. 2, the particles were covered in small agglomerations of silver particles not incorporated in the coatings. It may be that these free silver nanoparticles helped create the initial inter-particle contacts, if they were present in between the particles in the contact zones when the particles were pressed together during curing. Asperities due to the inherent surface roughness of the coatings may have had the same effect. Post-curing and thus further shrinkage of the epoxy matrix have been used to explain further decrease in resistivity of already cured flake-based ICAs during storage at elevated temperatures.[1] For most of the samples in this study, there was a slight decrease in measured *post-ET* thickness, on average between 1% and 3% for all the ICA series, suggesting that there may have been some shrinkage due to post-curing of the epoxy matrix. However, this is in the smallest range measurable by the digital callipers, so this shrinkage is not certain.

Effect of Varying Stiffness Behaviour

The mechanical behaviour of the AgPS should be more influenced by the properties of the polymer cores as the coating thickness decreases. The 60Ag particles were thus softer than the particles with thicker coatings, and it may be that this affected the stresses in the silver films as well as inter-particle pressure in a way that inhibited the formation of the metallurgical contacts. Gakkestad et al. reported the glass transition temperature ($T_{g,epoxy}$) of a cured epoxy system equal to the one used in these ICA samples to be around 78°C.[2] The glass transition ($T_{g,PMMA}$) of similar PMMA cores as the ones used in this study was reported as about 122°C. This is higher than the glass transition temperature normally reported for PMMA, which is around 105°C, although some authors have reported $T_{g,PMMA}$ around this temperature.[16] During the environmental test in this study, the chamber temperature was 85°C; above that of $T_{g,epoxy}$, but lower than $T_{g,PMMA}$. Below the glass transition temperature, the polymer cores will behave stiffer and the thermal expansion coefficient will be smaller. In addition, there is a balance in the epoxy matrix between thermal expansion and possible shrinkage due to post-curing. These are all factors that will affect the type and magnitude of stress in the silver coatings, as well as the inter-particle pressure. The complex interplay between the temperature-dependent properties of the polymer components and the formation and growth of the metallurgical connections during harsh environmental testing are not clear from the present data, and should be a topic for further investigation.

Electrochemical Ostwald Ripening at High Humidity

The mechanisms suggested in the previous sections do not take into account possible effects from the high moisture content during environmental testing. A possible explanation for the decreased resistivity *post-ET* could be at least partly electrochemical in nature. Redmond et al. described how larger silver nanoparticles grow on the detriment of smaller particles when the particles are immersed in water and in electrical contact through a conductive substrate.[23] Because of size-dependent shifts in the standard electrode potentials of nanoparticles, smaller particles are more easily oxidized than larger, setting up a larger concentration of silver ions (Ag^+) around the smaller particles at equilibrium. A similar size-dependent shift in the work function means that electrons can escape more easily from smaller particles. At equilibrium, this creates partial positive charges in the smaller particles and partial negative charges in the larger particles, drawing Ag^+ towards the larger particles. The ions are absorbed onto the larger particles, which re-establish electrical equilibrium by accepting electrons from the smaller particles through a conductive substrate, and the growth cycle continues. For AgPS-based ICAs the silver films could by themselves act as the conductive substrates. As long as Ag^+ can diffuse through the water-saturated polymer network, the electrochemical Ostwald ripening proposed by Redmond et al. is a possible mechanism for grain growth during the environmental test, which would help explain the decreasing resistivity values.

CONCLUSIONS

When the silver flakes of conventional isotropic conductive adhesive are replaced by micron-sized polymer spheres coated with tens to hundreds of nanometers of silver, the result is a complex composite system with a large range of factors influencing the material properties. Such ICAs yield resistivities similar to conventional ICAs while using only a fraction of the silver content, but the conduction mechanisms responsible for this effective use of silver have not yet been properly understood. In this work, we showed that for ICAs prepared with approximately the same volume fraction of particles, but different estimated coating thicknesses (60 nm, 100 nm, 150 nm, and 270 nm), the electrical resistivity decreased with increasing coating thickness. The resistivity also decreased for all four ICA series after storage for 3 weeks at 85°C/85% RH. FE-SEM imaging of ion milled ICA cross-sections revealed the nano-grained structure of the silver coatings and that metallurgical connections wider than the thicknesses of the films were formed at the inter-particle contacts. When such contacts are formed, the ICA bulk resistance will not be dominated by the contact resistance, but instead by the conductivity and thickness of the silver coatings. Possible mechanisms for the formation of metallurgical connections during adhesive curing and environmental testing were suggested. Increased inter-particle pressures due to curing of the epoxy and thermal expansion of the polymer cores is a likely mechanism. Grain growth owed to elevated temperatures and electrochemical Ostwald ripening at high moisture contents are also likely contributing factors. Further work to understand these mechanisms should thus include investigating the impact of various curing conditions, as well as de-coupling the influence of temperature and humidity on this composite system.

ACKNOWLEDGEMENTS

The Research Council of Norway is acknowledged for funding through Project Number 225962/E20—"Novel conductive adhesive technology for solar industry". Partial funding for this work was obtained from the Norwegian Ph.D. Network on Nanotechnology for Microsystems, which is sponsored by the Research Council of Norway, Division for Science, under Contract No. 221860/F40. Partial funding has also been obtained from the European Union Seventh Framework Programme FP7-NMP-

2013-LARGE-7 under Grant Agreement No 604668 ("Quantiheat") and by funding from the European Union Seventh Framework Programme (FP7/2007-2013) under Grant Agreement No FP7-NMP-310420 ("HyperConnect"). This work was supported by JSPS Core-to-Core Program, A. Advanced Research Networks. Hao Zhang and Jun Wang, both at The Institute of Scientific and Industrial Research, Osaka University, are gratefully acknowledged for their help with instrument training and sample preparation for SEM imaging. Lindberg & Lund AS (Vestby, Norway) are acknowledged for making available their adhesive lab for sample preparation. The authors of Ref. 2 are thankfully recognized for sharing their Thermal Mechanical Analyzer data on the epoxy matrix.

OPEN ACCESS

This article is distributed under the terms of the Creative Commons Attribution 4.0 International License (http://creativecommons.org/licenses/by/4.0/), which permits unrestricted use, distribution, and reproduction in any medium, provided you give appropriate credit to the original author(s) and the source, provide a link to the Creative Commons license, and indicate if changes were made.

REFERENCES

1. Y. Li, D. Lu, and C.P. Wong, *Electrical Conductive Adhesives with Nanotechnologies* (New York: Springer, 2010), pp. 121–225.
2. J. Gakkestad, Z. Li, T. Helland, and C.P. Wong, *IEEE Electron. Packag. Technol. Conf., 15th* (2013) doi:10.1109/EPTC.2013.6745715.
3. H.V. Nguyen, E. Andreassen, H. Kristiansen, and K.E. Aasmundtveit, *IEEE Trans. Comp. Packag. Manuf. Technol.* (2013). doi:10.1109/TCPMT.2013.2259166.
4. H.V. Nguyen, E. Andreassen, H. Kristiansen, R. Johannessen, N. Hoivik, and K.E. Aasmundtveit, *Mater. Des.* 46, 784 (2013).
5. S. Jain, D.C. Whalley, M. Cottrill, H. Kristiansen, K. Redford, C.B. Nilsen, T. Helland, and C. Liu, *Microelectronics and Packaging Conference (EMPC), 2011 18th European* (Brighton, UK 2011).
6. S. Jain, D.C. Whalley, M. Cottrill, H. Kristiansen, K. Redford, S. Helland, T. Helland, E. Kalland, and C. Liu, *Microelectronics Packaging Conference (EMPC), 2013 European* (Grenoble, France 2013).
7. S. Jain, D.C. Whalley, M. Cottrill, T. Helland, H. Kristiansen, K. Redford, and C. Liu, *IEEE Electron. Compon. Technol. Conf.* (2013). doi:10.1109/ECTC.2013.6575664.
8. G.R. Ruschau, S. Yoshikawa, and R.E. Newnham, *J. Appl. Phys.* 72, 953 (1992).
9. D. Lu, Q.K. Tong, and C.P. Wong, *Proc. Int. Symp. Adv. Packag. Mater.: Processes, Prop. Interfaces* (1999) doi: 10.1109/ISAPM.1999.757278.
10. R. Holm, *Electric Contacts: Theory and Application*, 4th ed. (Berlin: Springer, 2000), pp. 1–16, 118–134.
11. A.F. Mayadas and M. Shatzkes, *Phys. Rev. B* 1, 1382 (1970).
12. U. Kreibig and C.V. Fragstein, *Z. Phys.* 224, 307 (1969).
13. H. Jiang, K.S. Moon, J. Lu, and C.P. Wong, *J. Electron. Mater.* 34, 1432 (2005).
14. H. Jiang, K.S. Moon, Y. Li, and C.P. Wong, *Chem. Mater.* 18, 2969 (2006).
15. Y. Li, K.S. Moon, and C.P. Wong, *J. Appl. Polym. Sci.* 99, 1665 (2006).
16. J. Brandrup, E.H. Immergut, E.A. Grulke, A. Abe, and D.R. Bloch, *Polymer Handbook*, 4th edn. vol. 1. (Wiley, New York, 1999), pp. V/87, VI/203–VI/204.
17. D.R. Lide, *CRC Handbook of Chemistry and Physics*, 84th ed. (Boca Raton: CRC Press, 2003), pp. 12–220.
18. E.M. Petrie, *Epoxy Adhesive Formulations*, 1st ed. (New York: McGraw-Hill Education, 2006), pp. 57–58.
19. C. Oh, S. Nagao, T. Kunimune, and K. Suganuma, *Appl. Phys. Lett.* 104, 161603 (2014).
20. C. Oh, S. Nagao, and K. Suganuma, *J. Electron. Mater.* 43, 4406 (2014).
21. C. Oh, S. Nagao, T. Sugahara, and K. Suganuma, *Mater. Lett.* 137, 170 (2014).
22. C. Oh, S. Nagao, and K. Suganuma, *J. Mater. Sci.: Mater. Electron.* 26, 2525 (2015).
23. P.L. Redmond, A.J. Hallock, and L.E. Brus, *Nano Lett.* 5, 131 (2005).